Macromolecules
ARTICLE

Macromolecules **2010**, *43*, 3455–3464 **3455**
DOI: 10.1021/ma9023813

Wormlike Polymer Brush: A Self-Consistent Field Treatment

Mingge Deng,[†] Ying Jiang,*[,†,‡] Haojun Liang,*[,†] and Jeff Z. Y. Chen[‡]

[†]*CAS Key Laboratory of Soft Matter Chemistry, Department of Polymer Science and Engineering and Hefei National Laboratory for Physical Sciences at Microscale, University of Science and Technology of China, Hefei, Anhui 230026, P. R. China, and* [‡]*Department of Physics and Astronomy, University of Waterloo, Waterloo, Ontario, Canada N2L 3G1*

Received October 27, 2009; Revised Manuscript Received March 4, 2010

ABSTRACT: We investigate a homopolymer brush system on the basis of the wormlike-chain model, incorporating an Onsager-type interaction between polymer segments in the excluded-volume interaction. The model depends on the ratio between the total polymer length and the persistent length and a reduced grafting density as two basic parameters. Our numerical solutions to the self-consistent field theory are compared with scaling properties that can be deduced in various limits. In the limit of long chain and weak-to-moderate grafting density, our numerical results follow the scaling power law predicted by the classical-trajectory theory of a flexible polymer brush. In the limit of long chain and high grafting density, our numerical results show that the brush properties are comparable to the conformational properties of a nematic wormlike solution. In the limit of rod brush, our numerical results are consistent with the solution of a trial-function treatment from a previous mean-field theory.

1. Introduction

Consider the theoretical model consisting of polymer chains attached by one end to a flat substrate with the other end left free. The excluded volume in the system will force the polymers stretching away from the substrate, making a typical conformation known as a polymer brush. This simple yet fundamental model is applicable to a wide range of synthetic materials and processes as well as to a large class of phenomena in natural and living systems.[1−4] Theoretical and experimental studies of polymer brushes have been an intensive research field in the past several decades.[1,5−18]

The exact solution to the model of polymer brush grafted on a surface, based on the classical-trajectory approach of a Gaussian weight for grafted polymer chains and a mean-field treatment for the interaction between polymers,[9,11] is one of a few exceptional examples in soft condensed matter physics that demonstrates the beauty of theoretical treatment for a practical system. The resulting physical properties for the density profile, brush height, and free energy as functions of the polymer length, grafting density, and polymer−polymer interaction strength are in agreement with direct Monte Carlo computer simulations,[19−23] molecular-dynamics simulations,[15,24−27] and numerical solution to self-consistent field theories.[13,28−30] As well, theoretical predictions are consistent with experimental observations.[16,17,31]

Most biological molecules are more appropriately described by a wormlike-chain model, which has a number of interesting physical properties similar to and different from those of a Gaussian model, depending on the parameter regime of application; understanding the conformational properties of a wormlike polymer brush (see Figure 1) is a fundamental problem in soft condensed matter and biological physics. Moreover, the excluded-volume interaction between grafted wormlike polymers is expected to have an orientational dependence. In this work, we study the conformational properties of a homopolymer wormlike brush on the basis of the Saito−Takahashi−Yunoki model (STY),[32] which replaces the Gaussian weight previously used for the polymer statistics, and orientationally dependent Onsager interaction for polymer segment−segment excluded-volume interaction,[33] which replaces the orientationally independent interaction often used in previous studies. The same ingredients have been used in formulating models for related inhomogeneous wormlike systems in a self-consistent field treatment.[34−37,40,41] It is worth noting that in a 1979 article Jahnig already realized the importance of the wormlike brush problem and started formulating a theoretical treatment.[42] In terms of a Langmuir monolayer, Schmid also considered a similar model where polymer chains are made of connected rods with bending energy.[43] While the formalism of a self-consistent theory for a lyotropic wormlike brush is relatively straightforward (see section 2), to our best knowledge, no attempt has been made to solve such a model. Other approaches such as scaling argument[61] and computer simulations[23,28] are available.

The model established in this work for a wormlike brush is expressed in terms of two important parameters as will be explained in detail in section 2.2. The first is L/a, the ratio between the total contour length L of a wormlike chain and the effective Kuhn length a which can be identified with twice of the bare persistent length in the STY model.[32] This ratio becomes large for a flexible chain and small for a rodlike chain. Another is $\nu\sigma/a$, where σ is number of grafted chain per unit area on the grafting surface and ν the excluded-volume parameter. The conformational properties and free energy can be expressed as functions of these two parameters, as discussed in section 3.

One of the advantages of using a wormlike-chain model is its embedded mechanism of handling the finite maximum extensibility of a polymer chain of length L. In a moderately stretched brush, the average brush height, measured by the nongrafted end of polymers, scales linearly with the chain length L, as shown by both scaling theory[5,6] and classical-trajectory theory.[9−11] In high grafting density, one expect that the brush height approaches L as the upper limit. The lack of finite extensibility of a Gaussian model has been a concern, and a couple attempts have been made to revise the polymer brush theory.[44,45] Shim and Cates, for

*To whom correspondence should be addressed. E-mail: y35jiang@scimail.uwaterloo.ca (Y.J.); hjliang@ustc.edu.cn (H.L.).

Published on Web 03/18/2010

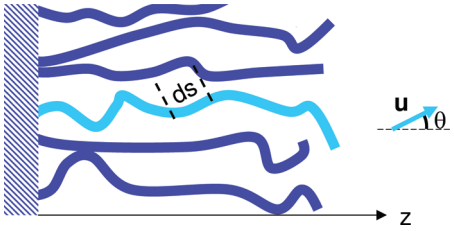

Figure 1. Sketch of the side view of a wormlike brush. The curves represent polymers, modeled here by cylindrical filaments, each having a total length of L and cross-section diameter d. A coordinate system is also shown where a polymer segment ds is specified by both distance from the surface, z, and the angle that it makes with respect to z, θ. An arc variable s, ranging from 0 at the grafting point to L at the polymer end, is used.

example, introduced a denominator to the Gaussian quadratic term, limiting the extensibility of a segment;[44] Lai and Halperin introduced the inverse of the Langevin function in lieu of the quadratic Gaussian term, enforcing an overall finite extensibility limit.[45] Both models used the Flory−Huggins expression to represent the free energy of volume interaction between polymer segments. As a result, they have shown that in the dense grafting region average brush height asymptotically approaches L as a linear function of the grafting density. This can be contrasted with our results below for wormlike brush made of long polymers, $L \gg a$, where the average brush height approaches L with a correction term inversely proportional to the grafting density by a power law. In another major difference, the contribution to the free energy per chain from the elastic energy diverges drastically, though in different forms, from these effective fixing of the Gaussian elastic energy,[44,45] while the wormlike brush model in this work yields a corresponding conformation energy contribution which diverges in a power law (see section 3.3).

Our formalism is also suitable for studying the problem of a rod brush formed by end-grafted rods on a surface, which was first examined by Jahnig.[42] Within a mean-field theory and also incorporating the Onsager interaction, Halperin, Alexander, and Schechter studied the directional ordering of such a system in terms of a trial-function approach;[46] in section 3.3 we see that the numerical results from our work are fully consistent with the prediction from this theory.

2. Theoretical Treatment for a Wormlike Polymer Brush

In this section we formulate the self-consistent field theory for a polymer brush consisting of monodisperse wormlike polymers, each having one end grafted to a flat impenetrable surface. The statistical weight of a polymer semiflexible polymer with a bending energy penalty is used[32] where both finite extensibility of the chain and segment orientation distribution are automatically incorporated. The normal to the surface is defined as the z-axis where the wall surface is represented by $z = 0$. The chains are uniformly grafted on the surface with a moderate to high grafting density σ. The expression for the interaction between the polymer segments is taken from a generalized Onsager interaction.

2.1. Self-Consistent Field Theory for a Wormlike-Chain System. The configuration of a particular grafted wormlike chain is described by a continuous space curve along which the arc variable s is specified: $s = 0$ at the grafted end and $s = L$ at the free end. For a particular polymer segment labeled s, both position vector $\mathbf{r}(s)$, which gives the spacial location, and unit vector $\mathbf{u}(s)$, which gives the tangent direction, are considered; these two variables are connected through a constraint

$$\mathbf{u}(s) = \mathrm{d}\mathbf{r}(s)/\mathrm{d}s \tag{1}$$

A further constraint is that $\mathbf{u}(s)$ is a unit vector, which is necessary not only to guarantee that the chain total extension is limited to L but also to prevent other potential unphysical problems.[47]

The characteristic length scale of a wormlike chain is its bare persistent length, which can be related to the bending energy of adjacent bonds in a typical wormlike-chain model. In a free space and in the absence of the excluded-volume interaction between polymer segments, a long wormlike chain also takes a random walk conformation, where twice of the bare persistent length can be identified with the Kuhn length.[32,47,48] In order to compare the physical properties of a brush deduced from a wormlike model to those from a Gaussian model, instead of the persistent length, we use such an effective Kuhn length, a, as a basic measure for a polymer segment throughout this paper.

One of the central physical quantities that we calculate in this work is the segmental distribution function $\phi(\mathbf{r},\mathbf{u})$, the number of effective Kuhn segments per unit volume at $\mathbf{r}$ and per solid angle in the direction $\mathbf{u}$. This distribution function follows the normalization condition

$$\int \mathrm{d}\mathbf{r}\, \mathrm{d}\mathbf{u}\, \phi(\mathbf{r},\mathbf{u}) = nL/a \tag{2}$$

where n is the number of grafted chain in the system. In a typical self-consistent field theory treatment employing a saddle-point approximation,[49] the system free energy nF can be written as

$$nF/k_{\mathrm{B}}T = -n \ln Q - \int \mathrm{d}\mathbf{r}\, \mathrm{d}\mathbf{u}\, W(\mathbf{r},\mathbf{u})\phi(\mathbf{r},\mathbf{u}) + \frac{1}{2}\int \mathrm{d}\mathbf{r}\, \mathrm{d}\mathbf{u}\, \mathrm{d}\mathbf{r}'\, \mathrm{d}\mathbf{u}'\, \phi(\mathbf{r},\mathbf{u})U(\mathbf{r},\mathbf{r}';\mathbf{u},\mathbf{u}')\phi(\mathbf{r}',\mathbf{u}') \tag{3}$$

where k_{B} is the Boltzmann constant, T temperature, Q the single-chain partition function, and $U(\mathbf{r},\mathbf{r}';\mathbf{u},\mathbf{u}')$ the interaction between two polymer segments located at $\mathbf{r}$ and $\mathbf{r}'$ and pointing in the directions of $\mathbf{u}$ and $\mathbf{u}'$. This free energy is accurate to the second-order virial approximation and contains a self-consistent field $W(\mathbf{r},\mathbf{u})$. We adopt the view that the grafting of the $s = 0$ end to a wall voids the indistinguishability of the chains that would give rise to a $1/n!$ in the front of the system partition function, hence yielding $-n \ln(nQ)$ in the first term. For tethered polymers with mobile $s = 0$ ends the inclusion of the additional $-n \ln n$ in the free energy is straightforward and does not influence the main results in this work. It is understood that the free energy as a functional of $W(\mathbf{r},\mathbf{u})$ and $\phi(\mathbf{r},\mathbf{u})$ needs to be minimized with respect to these two functions, in a saddle-point treatment.

In a typical bead−spring model for polymers where the excluded-volume interaction is usually characterized by the size of a bead, w, the interaction energy $U(\mathbf{r},\mathbf{r}';\mathbf{u},\mathbf{u}') = w\delta(\mathbf{r}-\mathbf{r}')$ and is independent of the orientation of $\mathbf{u}$ and $\mathbf{u}'$ of the two interacting polymer segments.[9] A wormlike chain with an embedded excluded-volume interaction can be regarded as a cylindrical filament characterized by a cross-sectional diameter d. We can readily use the Onsager expression,[33] within the second virial approximation, for the excluded interaction between polymer segments

$$U(\mathbf{r},\mathbf{r}';\mathbf{u},\mathbf{u}') = v\delta(\mathbf{r}-\mathbf{r}')|\mathbf{u}\times\mathbf{u}'| \tag{4}$$

where

$$v = 2da^2 \tag{5}$$

and terms of order d^2a and d^3 have been dropped. Minimization of the free energy (3) with respect to $\phi(\mathbf{r},\mathbf{u})$ gives an expression for the self-consistent field

$$W(\mathbf{r},\mathbf{u}) = v\int d\mathbf{u}'\,|\mathbf{u}\times\mathbf{u}'|\phi(\mathbf{r},\mathbf{u}') \tag{6}$$

The orientationally dependent, excluded-volume potential energy of such a form has been shown to be one of possible mechanisms driving liquid-crystal phase transitions in bulk wormlike polymers[50−52,55] and a number of orientationally dependent surface phase transitions in systems where a flat surface coexists with wormlike polymers.[36,40,56]

The first term of the system free energy in (3) contains a single-chain partition function Q, which can be calculated based on a wormlike chain model in the self-consistent field $W(\mathbf{r},\mathbf{u})$ and additional external field $V(\mathbf{r},\mathbf{u})$ representing the existence of the flat impenetrable surface. Following Saito, Takahashi, and Yuniki (STY),[32] for the probability distribution of a wormlike chain having configuration $\mathbf{u}(s)$ we write

$$P \propto \exp\left[-\int_0^L ds\left\{\frac{a}{4}\left|\frac{d\mathbf{u}(s)}{ds}\right|^2 + \frac{1}{a}(W[\mathbf{r}(s),\mathbf{u}(s)] + V[\mathbf{r}(s),\mathbf{u}(s)])\right\}\right] \tag{7}$$

where $\mathbf{r}(s)$ and $\mathbf{u}(s)$ are subject to the constraint (1). In replacement of the original bending energy coefficient $\beta\varepsilon$ in the first term of the exponent of the STY model,[32] we have explicitly included an effective Kuhn length a in the above, with the understanding that a is twice the bare persistent length, or, $a = 2\beta\varepsilon$, where $\beta\varepsilon$ is the reduced bending energy used in the original version.[32]

To facilitate the calculation of the partition function Q and the distribution function $\phi(\mathbf{r},\mathbf{u})$, we introduce the conditional probability, $q(\mathbf{r},\mathbf{u};s)$, for a grafted polymer portion of total arc length s which has an end located at $\mathbf{r}$ and pointing in the direction specified by the unit vector $\mathbf{u}$. It can be shown that under the constraint (1) the calculation of $q(\mathbf{r},\mathbf{u};s)$ following the probability (7) can be formulated into solving[47]

$$a\frac{\partial}{\partial s}q(\mathbf{r},\mathbf{u};s) = [\nabla_{\mathbf{u}}{}^2 - a\mathbf{u}\cdot\nabla_{\mathbf{r}} - W(\mathbf{r},\mathbf{u}) - V(\mathbf{r},\mathbf{u})]q(\mathbf{r},\mathbf{u};s) \tag{8}$$

with an appropriate grafting condition $q(\mathbf{r},\mathbf{u};s=0)$ to be specified below. In addition, a conjugate conditional probability satisfying the same differential equation, $q^*(\mathbf{r},\mathbf{u};s)$, is needed to complete the formalism. This is a probability for a polymer portion of total arc length s which has the end labeled s located at $\mathbf{r}$ and pointing in the direction specified by the unit vector $\mathbf{u}$ and an end labeled $s=0$ being left freely moving in space; the latter can be represented by an initial condition that will be specified below as well. Once these functions are obtained, we can calculate that the single-chain partition function

$$Q = \int d\mathbf{r}\int d\mathbf{u}\, q(\mathbf{r},\mathbf{u};s=L) \tag{9}$$

From the minimization of the free energy (3) with respect to $W(\mathbf{r},\mathbf{u})$, one has

$$\phi(\mathbf{r},\mathbf{u}) = \frac{n}{aQ}\int_0^L ds\, q(\mathbf{r},\mathbf{u};s)q^*(\mathbf{r},-\mathbf{u};L-s) \tag{10}$$

The derivation of (8) and (9) starting from (3) is a standard procedure in the self-consistent mean-field theory of polymers.[49] The modified diffusion equation (8) together with expressions (6), (9), and (10) completely form a self-consistent set, which need to be solved for a wormlike-chain problem.

It is worth noting that in an early treatment of lipid membrane molecules[42] Jahnig actually used a statistical weight incorporating a bending energy between adjacent polymer segments, that is, an energy penalty similar to the first term in the exponent of (7). This approach allowed him to handel long flexible and short rodlike chains. No coupling between the $\mathbf{r}$ and $\mathbf{u}$ vectors was considered, and the interaction term, W, was also oversimplified.

2.2. Formalism for a Wormlike Brush. In this section, we exploit the planar symmetry in the current system, using a z coordinate for the position of a polymer segment and θ angle to represent the projection of the unit vector $\mathbf{u}$ onto the z-axis. In addition, we define reduced variables

$$\bar{z} \equiv z/a \tag{11}$$

$$\bar{s} \equiv s/a \tag{12}$$

The equation set in the last section can then be written in a simplified version, enabling us to perform numerical solution.

The distribution functions q and q^*, for example, are only dependent on $\bar{z}$, θ, and $\bar{s}$; the modified diffusion equation in (8) can be rewritten as

$$\frac{\partial}{\partial\bar{s}}q(\bar{z},\theta;\bar{s}) = \left[\frac{1}{\sin\theta}\frac{\partial}{\partial\theta}\sin\theta\frac{\partial}{\partial\theta} - \cos\theta\frac{\partial}{\partial\bar{z}} - W(\bar{z},\theta) - V(\bar{z},\theta)\right]q(\bar{z},\theta;\bar{s}) \tag{13}$$

The initial condition $q(\bar{z},\theta;\bar{s}=0)$ needed for solving this differential equation is given by

$$q(\bar{z},\theta,0) = \begin{cases}\delta(\bar{z}) & \text{if } \cos\theta > 0\\ 0 & \text{otherwise}\end{cases} \tag{14}$$

which represents a uniform grafting layer of $\bar{s}=0$ ends at the plane $\bar{z}=0$. Note that this initial condition contains an angular dependence, reflecting the fact that the orientation of the initially grafted polymer segments can only be in the positive z direction. The function q^* satisfies the same differential equation, where the initial condition is given by

$$q^*(\bar{z},\theta,0) = \begin{cases}1 & \text{if } \bar{z}>0 \text{ or } \bar{z}=0 \text{ and } \cos\theta<0\\ 0 & \text{otherwise}\end{cases} \tag{15}$$

As well, there is a directional dependence in the above. These initial conditions can be compared with their counterparts in the self-consistent field theory treatment of a Gaussian polymer brush,[13] where there is no direct involvement of the direction. The potential function V in the differential equation also contains an angular dependence

$$V(\bar{z},\theta) = \begin{cases}0 & \text{if } \bar{z}>0 \text{ or } \bar{z}=0 \text{ and } \cos\theta\le 0\\ \infty & \text{otherwise}\end{cases} \tag{16}$$

which has been previously introduced to describe a featureless hard wall in other wormlike-chain systems.[40,56−58]

Taking (9) and defining $\bar{Q} \equiv Q/(Aa)$, we have the reduced single chain partition function per unit area

$$\bar{Q} = 2\pi \int \mathrm{d}\bar{z} \int \mathrm{d}\theta \sin\theta q(\bar{z},\theta;\bar{s} = L/a) \quad (17)$$

where A is the total grafting area. With that, the density profile ϕ in (10) can be determined; instead of ϕ itself, in our calculation we use $\rho(\bar{z},\theta) \equiv \phi(\mathbf{r},\mathbf{u})/\sigma$, the per-chain number density of polymer segments located at $\bar{z}$ and pointing within a unit solid angle about θ

$$\rho(\bar{z},\theta) = \frac{1}{\bar{Q}} \int_0^{L/a} \mathrm{d}\bar{s}\, q(\bar{z},\theta;\bar{s}) q^*(\bar{z},\pi-\theta;L/a-\bar{s}) \quad (18)$$

This means that ρ satisfies the normalization condition

$$2\pi \int_0^{\infty} \mathrm{d}\bar{z} \int_0^{\pi} \mathrm{d}\theta \sin\theta\, \rho(\bar{z},\theta) = L/a \quad (19)$$

Returning to the expression for the self-consistent field, W in (6), we complete the self-consistency by writing

$$W(\bar{z},\theta) = (v\sigma/a) \int_0^{2\pi} \mathrm{d}\varphi' \int_0^{\pi} \mathrm{d}\theta' \sin\theta' |\mathbf{u}\times\mathbf{u}'| \rho(\bar{z},\theta') \quad (20)$$

where $|\mathbf{u}\times\mathbf{u}'| = (1-\cos^2\gamma)^{1/2}$ and $\cos\gamma = \cos\theta\cos\theta' + \sin\theta \sin\theta'\cos\varphi$. Once self-consistent field equations, eqs 8, 17, 18 and 20, are solved and a numerical procedure for solving these converges, the free energy per chain becomes

$$\beta F = -\ln\bar{Q} - \pi \int_0^{\infty} \mathrm{d}\bar{z} \int_0^{\pi} \mathrm{d}\theta \sin\theta\, W(\bar{z},\theta)\rho(\bar{z},\theta) \quad (21)$$

These equations, eqs 13 and 17−21, form a self-consistent set. The numerical method used in solving this equation set is presented below, and the solution of this set is presented in the next section.

2.3. Numerical Scheme. In the numerical solution to the theory developed above we paid attention to the functions $q(\bar{z},\theta,\bar{s})$ and $q^*(\bar{z},\theta,\bar{s})$, where all three variables, $\bar{z}$, θ, and $\bar{s}$, are treated in direct discretization. The main steps of the algorithm used for solving the equations consistently are listed below.

(a) Initially, to obtain a solution of a weak $v\sigma/a$ system, we used a parabolic profile as an initial guess. Otherwise, the initial condition for the field $W(\bar{z},\theta)$ is made as a function of $\bar{z}$ and θ, taken from an existing solution of a similar physical condition (i.e., similar $v\sigma/a$ and a/L).

(b) The modified diffusion equations for $q(\bar{z},\theta,\bar{s})$ and $q^*(\bar{z},\theta,\bar{s})$ are solved along the entire contour length, from $\bar{s} = 0$ to $\bar{s} = L/a$, step by step, according to an implementation of the Crank−Nicholson scheme[59] coupled with an alternating-direction implicit method. The step length for $\bar{s}$ is taken as $\mathrm{d}\bar{s} = 0.01$, where $q(\bar{z},\theta,0)$ and $q^*(\bar{z},\theta,0)$ in (14) and (15), respectively, are used as the initial conditions. In numerical implementation, instead of grafting the polymer at $\bar{z} = 0$ (i.e., use a delta function $\delta(\bar{z})$), we actually used an initial condition that corresponds to grafting the polymer at $\bar{z} = \varepsilon$ from the substrate, $\delta(\bar{z}-\varepsilon)$, where $\varepsilon = 0.01$ is a small number. This numerical trick avoids a potential divergence of the algorithm and has been used previously.[30] The derivatives on the right-hand side of eq 13 are expressed by a central difference scheme, where the step length $\mathrm{d}\bar{z} = 0.01$ and $\mathrm{d}\theta = \pi/30$ are taken for the variable $\bar{z}$ and θ, respectively.

(c) Once the probability distribution functions $q(\bar{z},\theta,\bar{s})$ and $q^*(\bar{z},\theta,\bar{s})$ are determined, we evaluate the monomer densities $\rho(\bar{z},\theta)$ according to (18), using Simpson's rule for the integration over the variable $\bar{s}$.

(d) We then update the self-consistent field $W(\bar{z},\theta)$ using a Picard iteration method

$$W_{\mathrm{new}}(\bar{z},\theta) = W_{\mathrm{old}}(\bar{z},\theta) + \lambda[(v\sigma/a) \int_0^{2\pi} \mathrm{d}\varphi' \int_0^{\pi} \mathrm{d}\theta' \sin\theta' |\mathbf{u}\times\mathbf{u}'| \rho(\bar{z},\theta') - W_{\mathrm{old}}] \quad (22)$$

(e) The iteration factor λ is fixed at a small value $\lambda = 0.1$.

(f) Having obtained the new self-consistent field $W_{\mathrm{new}}(\bar{z},\theta)$, we go back to step b for iterations. The numerical procedure continued until the convergence criterion imposed on the field was satisfied, Max $|W_{\mathrm{new}} - W_{\mathrm{old}}| < 10^{-5}$.

3. Results and Discussion

In this section we discuss the characteristics of a wormlike polymer brush. There are only two relevant combinations of parameters in the equation system, eqs 13 and 17−21, that is, $v\sigma/a$ and L/a, reduced surface grafting density and total number of segments in a chain. At first glance, this bears a similarity to the self-consistent field theory of a Gaussian polymer brush[9,10] where the same combinations of parameters appears. The latter, however, actually contains one combination of parameters that was shown to be important (see the definition of the so-called β_{NS} parameter[13]). The two independent parameters in a wormlike polymer brush problem in this work yield much richer conformational behavior than a Gaussian model, to be discussed below.

We have obtained numerical solutions for the distribution function and the free energy in a wide range of parameters $v\sigma/a$ and L/a, covering interesting limits and the crossover between them. Figure 2 presents the numerical results for the free energy per chain, $F(v\sigma/a,L/a)$, scaled by $\beta a/L$, as a function of the reduced grafting density $v\sigma/a$ for various values of L/a.

On the basis of the numerical computation of the distribution function for segments of Kuhn length a, $\rho(\bar{z},\theta)$, we obtained the average segment-to-surface distance $\langle\bar{z}(v\sigma/a,L/a)\rangle$

$$\langle\bar{z}\rangle \equiv \frac{\int_0^{\infty}\mathrm{d}\bar{z}\int_0^{\pi}\mathrm{d}\theta\sin\theta\,\bar{z}\rho(\bar{z},\theta)}{\int_0^{\infty}\mathrm{d}\bar{z}\int_0^{\pi}\mathrm{d}\theta\sin\theta\,\rho(\bar{z},\theta)} \quad (23)$$

which is displayed in Figure 3A. The segmental distribution function also allows us to characterize the average orientational order of segments, measured by

$$\langle S_m\rangle = \frac{\int_0^{\infty}\mathrm{d}\bar{z}\int_0^{\pi}\mathrm{d}\theta\sin\theta\,P_m(\cos\theta)\rho(\bar{z},\theta)}{\int_0^{\infty}\mathrm{d}\bar{z}\int_0^{\pi}\mathrm{d}\theta\sin\theta\,\rho(\bar{z},\theta)}, \quad m = 1,2,\ldots \quad (24)$$

where $P_m(\cos\theta)$ is the Legendre polynomial of the mth rank. Plots C and D in Figure 3 present the first two orientational order parameters, $S_1(v\sigma/a,L/a)$ and $S_2(v\sigma/a,L/a)$, as functions of the reduced grafting density $v\sigma/a$. As for the density distribution function itself, we have plotted the angularly averaged density

$$\rho_0(\bar{z}) \equiv 2\pi \int_0^{\pi} \mathrm{d}\theta \sin\theta\, \rho(\bar{z},\theta) \quad (25)$$

as a function of z/a in Figure 4A for $L/a = 30$ and various values of $v\sigma/a$.

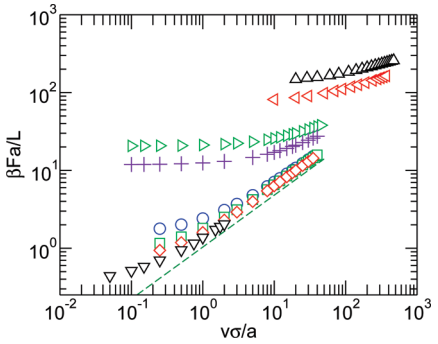

Figure 2. Free energy per chain per segment $\beta Fa/L$ of a wormlike brush as a function of the reduced grafting density $\nu\sigma/a$. Down triangles, diamonds, squares, circles, crosses, right triangles, left triangles, and upper triangles represent our numerical solution for L/a = 50, 30, 20, 10, 1, 0.5, 0.1, and 0.05, respectively. The long dashed line represents a slope of 2/3, appearing in the exponents of power laws (36) and (42).

Our calculation also produces the distribution function of the free end $q(\bar{z}, \theta; \bar{s} = L/a)$. To measure the average brush height $\langle \bar{z}_{\text{end}}(\nu\sigma/a, L/a)\rangle$, we use

$$\langle \bar{z}_{\text{end}}\rangle = \frac{\int_0^\infty d\bar{z} \int_0^\pi d\theta \sin\theta\, \bar{z} q(\bar{z}, \theta, \bar{s} = L/a)}{\int_0^\infty d\bar{z} \int_0^\pi d\theta \sin\theta\, q(\bar{z}, \theta; \bar{s} = L/a)} \tag{26}$$

which is displayed in Figure 3B. The end distribution function itself, averaged over angular dependence

$$g(\bar{z}) \equiv 2\pi \int_0^\pi d\theta \sin\theta\, q(\bar{z}, \theta; \bar{s} = L/a) \tag{27}$$

is plotted in Figure 4B for L/a = 30 and various values of $\nu\sigma/a$.

Next, we analyze these numerical results in a number of interesting limits. In the long-chain limit, $L/a \gg 1$, we expect to see that some properties of a Gaussian polymer brush recover in the moderate stretching region, $\nu\sigma/a \leq 1$ (see section 3.1); however, the built-in total stretching limit of a wormlike polymer in the formalism, L, and the effect of the Onsager interaction, (20), produce different scaling behavior in the high-grafting parameter region $\nu\sigma/a \gg 1$ (see section 3.2). As well, the formalism in this section allows us to examine rodlike polymer brush in the limit (see section 3.3), $L/a \ll 1$, and the crossover between short- and long-chain brushes.

3.1. Long-Chain $L/a \gg 1$ and Moderate Grafting $\nu\sigma/a \leq 1$. We generally expect that the physical properties of a wormlike-chain model recover those of a Gaussuan-chain model in the long chain limit

$$L/a \gg 1 \tag{28}$$

In particular, an interesting question is in which parameter region we recover the power-law scaling function

$$\langle z\rangle/L \propto \langle z_{\text{end}}\rangle/L \propto (\nu\sigma/a)^{1/3}, \quad L/a \gg 1 \tag{29}$$

which is well-known in the field.

It is essential to note that this scaling behavior, deduced from an Alexander analysis[5,48] or the classical-trajectory theory,[9,10] requires the fact that grafted brushes have significant overlapping over each other beyond the so-called mushroom region.[48] This can be deduced from the simple view that the brush hight must be greater than the radius of gyration, $\langle z\rangle \geq a(L/a)^{\nu_0}$, which, by taking (29), gives

$$(\nu\sigma/a)(L/a)^{\zeta} \geq 1 \tag{30}$$

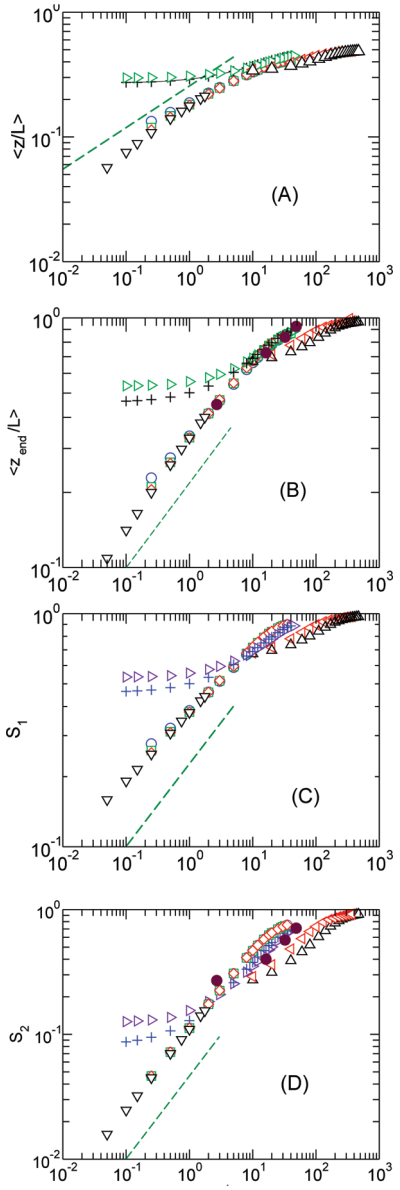

Figure 3. Mean end-monomer-to-grafting surface distance $\langle z_{\text{end}}\rangle$, mean monomer-to-grafting surface distance $\langle z\rangle$, and orientational order parameters S_1 and S_2 of a wormlike brush as functions of the reduced grafting density $\nu\sigma/a$. Down triangles, diamonds, squares, circles, crosses, right triangles, left triangles, and upper triangles represent our numerical solution for L/a = 50, 30, 20, 10, 1, 0.5, 0.1, and 0.05, respectively. Lines in (A) to (C) represent the exponents in power laws (29) and (37), with the identification in (35). In (B) and (D) we have also added the results from molecular dynamics simulations[38] by filled circles.

where the exponent $\zeta = 3 - 3\nu_0$ and the ν_0 is the radius-of-gyration exponent. Note that the left-hand side is simply $\beta_{\text{NS}}{}^{3/2}$ where β_{NS} is the sole parameter relevant in a Gaussian mean-field theory, defined by Netz and Schick[13] after taking $\nu_0 = 1/2$, which is appropriate at that level of theoretical approximation (giving $\zeta = 3/2$). One can also produce a requirement, taking the view that the distance between the grafted chains should be shorter than the radius of gyration, $\sigma^{-1/2} \leq a(L/a)^{\nu_0}$. Letting $\nu \sim a^3$—an approximation that can be taken by considering a flexible polymer but not the cylindrical filament considered in this work—one can show that the above requirement is also valid provided $\zeta = 2\nu_0$. Kent et al., for example, have introduced such an expression, using $\nu_0 = 3/5$, and hence $\zeta = 6/5$, as the criterion of when the brush limit following (29) is valid.[16]

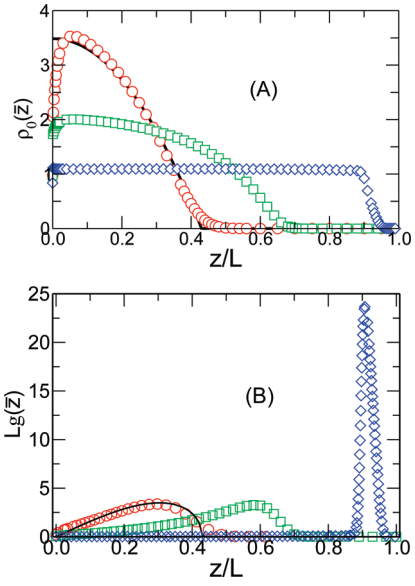

Figure 4. (A) Normalized density distribution function $\rho_0(\bar{z})$ and (B) normalized end distribution function $Lg(\bar{z})$ obtained from our numerical solution for a wormlike-brush model made of polymers having $L/a = 30$. Circles, squares, and diamonds correspond to reduced grafting densities $\nu\sigma/a = 0.25$, 2.0, and 35.0. The exact solution of a Gaussian brush based on a classical-trajectory approach[9,11] is also displayed by the solid curve for comparison, which is valid in the limit of $\nu\sigma/a \ll 1$.

Regardless of which requirement to take, qualitatively, we have a lower bound of $\nu\sigma/a$ for the validity of (29)

$$\nu\sigma/a \geq (L/a)^{-\zeta} \tag{31}$$

where ζ is either 6/5 in ref 16 or 3/2 in ref 13. In Figure 3A,B we have plotted a long-dashed line, which represents the 1/3 exponent predicted in (29) in a double-logarithmic plot. Our numerical data point in the small-$\nu\sigma/a$ regime for large L/a are seen to approach this asymptotic behavior. Furthermore, we can also observe how the scaling power law breaks down in the low $\nu\sigma/a$ region: small-L/a systems plateau out from the anticipated scaling law earlier than large-L/a systems, fully consistent with the criterion in (31) and the discussions in refs 13 and 16.

The wormlike polymer brush, however, has another restriction which does not appear in the Gaussian polymer brush, both within the self-consistent field theory treatment. We know that in extremely high stretching, because of the finite extensibility in wormlike chain, $\langle z \rangle$ cannot go beyond L. As a matter of fact, in order to observe a scaling relation in (29) which would state that $\langle z \rangle$ increases indefinitely, we must restrict ourself to the parameter region $\langle z \rangle \leq L$ (or, more restrictly, $\langle z \rangle \ll L$) for a wormlike brush. The use of (29) hence gives us another restriction, an upper bound

$$\nu\sigma/a \leq 1 \tag{32}$$

which needs to be considered for a wormlike brush. Note that in a Gaussian brush theory such an upper bound does not exist—Netz and Schick for example have recently shown that (30) is the only requirement that a Gaussian brush theory produces the scaling relation in (29). In wormlike brush, the upper bound (32) is not in conflict with the lower bound in (31) as L/a must be large to recover (29).

Having established that there is an upper bound in a wormlike brush, we can also observe from Figure 3A,B that the agreement between the 1/3 slope and the numerical data starts to break down approximately when $\nu\sigma/a$ is greater than 1. In other words, the scaling relation in (29) is valid only for moderate grafting density $\nu\sigma/a \leq 1$, provided that the chain length is long enough, in a wormlike brush. This is in contrast with the properties of a Gaussian chain, where only the lower bound exists.[13]

In order to facilitate the comparison of our results and those from a recent molecular dynamics simulations, we have related our definition of $\nu\sigma/a$ with the grafting density d in ref 38 by $\nu\sigma/a = 135.0d$. The numerical coefficient was adopted through comparing the normalized brush height of the first data point in Figure 4d of ref 38 with ours. The four data points, represented in Figure 3B by filled circles, agree well with our calculation.

Within the scaling region, the classical-trajectory theory also produces density profiles $\rho_0(\bar{z})$ and $g(\bar{z})$ in the scaling regime[9]

$$\rho_0(\bar{z}) = \frac{3}{2}\frac{L}{H}\left[1 - \left(\frac{z}{H}\right)^2\right] \tag{33}$$

$$g(\bar{z}) = \frac{3z}{H^2}\sqrt{1 - \left(\frac{z}{H}\right)^2} \tag{34}$$

where $H = (4\sigma w/\pi^2)^{1/3} L a^{-1/3}$. Note that $\rho_0(\bar{z})$ satisfies the normalization condition (19) and that $g(\bar{z})$ satisfies $\int \mathrm{d}z\, g(\bar{z}) = 1$. To compare with this prediction, we have identified

$$w = \pi v/4 \tag{35}$$

through equating the second term on the right-hand side of (3) for a **u**-independent density distribution with expression (3) in Milner et al.[9] These predictions are plotted as functions of z/L in Figure 4 by solid curves. For comparison, we have overlaid our numerical solution, represented by various symbols on top of the curves. Asymptotically, our numerical results for $\rho_0(\bar{z})$ and $g(\bar{z})$ at $L/a = 30$ and $\nu\sigma/a = 0.25$ (circles) are in agreement with these predicated functions. The deviation from the solid curve near the tail of the profile can be attributed to the fact that the approximation made in the classical-trajectory theory ignores trajectory fluctuations, which are more dominating in a low-density region. The orientationally dependent boundary condition near the wall in the current wormlike polymer brush problem 16, and the numerical trick of treating the grafted end at a small distance from the wall contribute to the deviation of the calculated profile from the above prediction. Similar deviations were seen in other full self-consistent field calculations for a polymer brush problem.[12,13]

At a relatively high density, say, $\nu\sigma/a = 2.0$ for $L/a = 30$ (squares in Figure 4A), we can see that the monomer density as a function of z/L begins to reflect a sharper drop than the parabolic profile. This is a crossover region where the brush height also starts to deviate from the scaling relationship in (33) and (34). A similar trend of the density profile change can be found in ref 38, where a molecular dynamics simulation has been conducted on a wormlike brush system; while the density profile agrees with (33) and (34) at low grafting density, deviation can be found approximately in the range $d = [0.12, 0.37]$, where d is the grafting density defined in ref 38. This is fully consistent with our assessment of the existence of an upper bound (32) in wormlike brush. Note that at this "high" value of $\nu\sigma/a$ for $L/a = 30$ a Gaussian brush still follows the power law, as demonstrated in Netz and Schick.[13]

A comparison between the free energy per grafted chain predicted by the classical-trajectory theory[9,11]

$$\beta F = \frac{9L}{40a}\left(\frac{4\pi\sigma w}{a}\right)^{2/3} \quad (36)$$

and our numerical data is made in Figure 2. The long-dashed line represents the 2/3 power-law exponent from this prediction. The agreement between the numerical results and the long-dashed line in Figure 2 can be viewed by a general trend that larger L/a data in the small $\nu\sigma/a$ regime asymptotically approach the predicted slope.

In a classical-trajectory theory, a polymer in a brush is always directed away from the grafting surface. The projection of a segment onto the z axis is related to cos θ; hence, on average

$$S_1 = \langle \cos\theta \rangle \propto \langle z_{\text{end}} \rangle / L \propto (\nu\sigma/a)^{1/3} \quad (37)$$

in the moderate stretching regime, $\nu\sigma/a \leq 1$, $L/a \gg 1$. We can see in Figure 3C that our numerical results for S_1 calculated from (24) indeed asymptotically follow this power law in the region of interest. The power law for S_1 in (37) was previously verified by computer simulations independent of the classical-trajectory theory[21,24] and by a mean-field Monte Carlo approach.[60]

In Figure 3D we have also displayed our numerical results for S_2 as a function of $\nu\sigma/a$, which, in the parameter region interested in this subsection, approaches a slope of 2/3 in the double-logarithmic plot. In fact, our data for higher order parameter S_m (not shown) indicates that

$$S_m = \langle P_m(\cos\theta) \rangle \propto (\nu\sigma/a)^{m/3}, \quad \nu\sigma/a \ll 1 \quad (38)$$

are generally followed. According to the classical-trajectory theory, however, we would arrive at the same 1/3 exponent for all S_m. Because orientational fluctuations are completely ignored in a classical-trajectory theory, we do not expect that the 1/3 scaling exponent from such a treatment would be correct for $m \geq 2$. It is highly desirable to *analytically* validate the above formula (38) for a wormlike brush. Except for the first data point, results of molecular dynamics simulations,[38] represented in Figure 3D by symbol filled circle, agree well with our calculation.

3.2. Long Chains $L/a \gg 1$ and High Grafting Density $\nu\sigma/a \gg 1$. At an extremely high grafting density, $\nu\sigma/a \gg 1$, the angularly averaged density profile (25) asymptotically approaches a step function, having a constant value in most region of z ($z < L$). Meanwhile, the angularly averaged distribution function of the free end shows a sharp peak at $z = L$, vanishing in most other regions of z ($z < L$). To illustrate this behavior, using diamond symbols, we plotted these distributions for a high density case, $\nu\sigma/a = 35$, as functions of z/L in Figure 4.

This step function profile is in agreement with various simulation studies[38,62] and is a sign that a self-consistent theory based on a Gaussian theory breaks down in this region of parameter. Repairing to a Gaussian theory often takes both finite extensibility and higher-order interaction terms beyond the second virial coefficient.[44,45] We have shown here that the finite extensibility of the wormlike formalism naturally gives a step function profile at high grafting density, even at the level of the second virial coefficient.

In this article, we deal with a brush made of polymer of cylindrical filaments of diameter d (see eq 5), the combination of parameters $\nu\sigma/a \approx 2da\sigma$. In systems like DNA array,[53,54] chains are densely grafted, to the maximal extent that $\sigma \sim 1/d^2$. Hence, $\nu\sigma/a$ can reach as high as $2a/d$, where a, twice of the persistence length which is ~500 Å in dsDNA, is much greater than the diameter d, that is, in the subnanometer region.[54] As a result, $\nu\sigma/a$ can be a large parameter.

Because the grafted chains are highly stretched at a large $\nu\sigma/a$, within the brush the structure of wormlike chains is similar to a nematic liquid-crystal phase of lyotropic polymers at a similar segmental density. For a wormlike polymer system, the analysis of both entropy penalty caused by orientational ordering and free energy due to the same Onsager excluded-volume interaction (6) were well established previously in trial-function approaches[50,51] and verified by the numerical solution to an equation similar to eq 8.[55] Using $\nu\sigma/a$ as the reduced segmental density in a strong nematic phase and adopting a result from Odijk,[51] we have

$$\langle \theta^2 \rangle \propto (\nu\sigma/a)^{-2/3}, \quad \nu\sigma/a \gg 1 \quad (39)$$

Because the orientational distribution is strongly peaked at $\theta = 0$, we have $1 - S_m \propto \langle \theta^2 \rangle$; hence, we expect

$$1 - S_m \propto (\nu\sigma/a)^{-2/3}, \quad \nu\sigma/a \gg 1 \quad (40)$$

where the proportional coefficient may have an m-dependence. Figure 5B shows that the expected power law above represented by a long-dashed straight line agrees with our numerical results represented by various symbols, for $m = 1, 2$.

One notable feature of the plots in Figures 3 and 5 is the lack of any signature of an isotropic−nematic phase transition; such a first-order phase transition is seen in bulk lyotropic wormlike polymer solutions with a similar range of segmental density, driven by the Onsager interaction.[50,51,55] In a lyotropic wormlike brush, an orientational ordering already exists at weak and moderate densities (see the last subsection), required by the fact that polymer chains must be stretched away from the grafting wall. As the grafting density (hence the segmental density) increases, significant orientational ordering is already yielded before the anticipated phase transition occurs in the bulk liquid-crystal phase. This result is in agreement with a scaling analysis of wormlike polymer brush in the long chain limit.[61] A Monte Carlo simulation of wormlike polymer brushes also shows that S_2 varies smoothly over a significant range of grafting density, although the authors claimed that a *phase transition* exists in an extremely small grafting region;[23] in our opinion, the weak orientational ordering in this region, shown in Figure 11 of ref 23 , is simply the initial development of orientational ordering in a brush.

The scaling behavior in (40) also allows us to estimate

$$1 - \frac{\langle z_{\text{end}} \rangle}{L} \propto \frac{1}{2} - \frac{\langle z \rangle}{L} \propto 1 - \langle \cos\theta \rangle \propto \left(\frac{\nu\sigma}{a}\right)^{-2/3} \quad (41)$$

for $\nu\sigma/a \gg 1$, where the last step was made in reference to (39). To demonstrate the validity of these power laws (41) in the strong stretching region, we plot both $1 - \langle z_{\text{end}} \rangle/L$ and $1/2 - \langle z \rangle/L$ using $a/\nu\sigma$ as the variable in Figure 5A. The anticipated power law is indicated by a straight line which agrees well with the asymptotic behavior of our numerical results represented by symbols for $1 - \langle z_{\text{end}} \rangle/L$. The numerical data of $1/2 - \langle z/L \rangle$ approaches the expected slope at small $\nu\sigma/a$. We note that the numerical errors of these data are of order 0.01 in the vertical scale. In the case of $1/2 - \langle z/L \rangle$, it is unclear whether the scaling law can be approached by considering even smaller $\nu\sigma/a$ or the scaling law has already been approached within the numerical errors.

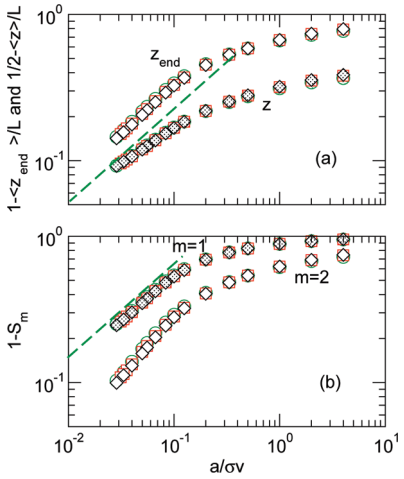

Figure 5. Behavior of $1/2 - \langle\langle z/L\rangle$ [open symbols in (a)], $1 - \langle z_{end}/L\rangle/L$ [filled symbols in (a)], $1 - S_1$ [filled symbols in (b)], and $1 - S_2$ [open symbols in (b)] as functions of $a/\sigma\nu$. Circles, squares, and diamonds represent our numerical solutions for $L/a = 10$, 20, and 30, and straight lines demonstrate the exponents in power laws (41) and (40).

Finally, we turn to the discussion of the free energy itself. Because of the analogy to a nematic phase in the strongly stretched limit, we can directly quote a known scaling result[51]

$$\beta F \propto \left(\frac{L}{a}\right)\left(\frac{\nu\sigma}{a}\right)^{2/3} \tag{42}$$

for $\nu\sigma/a \gg 1$. The crossover from moderate to strong stretching can be viewed from, for example, $\langle z_{end}\rangle/L$ data points in Figure 3, occurring within the region $\nu\sigma/a \sim [1, 10]$, in a double-logarithmic plot. The free energy itself, however, displays power laws (36) and (42) characterized by the same scaling exponent 2/3 in the entire region covered by our numerical solution (see Figure 2). In principle, there could be a difference in the coefficients of these power laws; this difference, however, is not visible in the series of symbols shown in Figure 2. Our numerical observation in this work for the first time demonstrates the possibility of a single power law for the free energy over the entire range of grafting density; it would be worthwhile to develop a physical argument that a single free-energy expression, including the same prefactor coefficient, is valid for both large and small $\nu\sigma/a$.

The behavior of the free energy for a wormlike brush can be contrasted with that of a single wormlike chain confined in a tube of radius R. At a large R/a, the power law for the free energy of a confined chain can be written as $\beta F \sim (L/a)(w/aR^2)^{2/3}$.[48] At a small R/a, the free energy of a long wormlike polymer confined in a tube displays the Odijk power law, $\beta F \sim (L/a)(aR)^{1/3}$,[51,63] with a completely different scaling exponent.

3.3. Brush of Rods $L/a \ll 1$ at High Grafting Density $\nu\sigma L/a^2 \geq 1$. In this subsection, we focus on the analysis of the numerical results in the parameter region where the persistent length $a/2$ is much greater than the total contour length L. Our physical problem, then, is reduced to surface grafted rods with weak flexibility. As was originally discussed by Onsager and will be shown below for a rod brush, in the rod limit, the excluded-volume interaction between two rods, of order L^2d, begins to play an important role when it becomes comparable to the volume of the space occupied by a rod, in our case, L/σ. Hence, the rod brush region considered in this subsection is governed by $L^2d \geq L/\sigma$ or $\nu\sigma L/a^2 \geq 1$ because of eq 5.

Based on the solution to eq 13, numerical results of $1 - \langle z_{end}\rangle/L$, $1/2 - \langle z\rangle/L$, S_1, and S_2 for chain length $L/a = 1$, 0.5, 0.1, and 0.05 are displayed in Figure 6 as a function of $a^2/\nu\sigma L$. As L/a becomes small (i.e., the wormlike polymer becomes more rodlike), the data in the four plots asymptotically approach the solid curves, representing the physical properties in the limit of a rigid-rod brush. Also plotted are dashed lines, representing the asymptotic scaling power laws, which will be discussed below.

In the rigid-rod limit, presented in our model by taking $a \gg L$, the basic length scale L becomes relevant, and the persistent length a is expected to drop out from the formalism. This can be explicitly demonstrated by introducing the definition

$$\tilde{z} = z/L \tag{43}$$

$$\tilde{s} = s/L \tag{44}$$

so that eq 13 now becomes

$$\frac{\partial}{\partial\tilde{s}}\, q(\tilde{z}, \theta; \tilde{s}) = \left[-\cos\theta\frac{\partial}{\partial\tilde{z}} - \tilde{W}(\tilde{z}, \theta) - \tilde{V}(\tilde{z}, \theta)\right] q(\tilde{z}, \theta; \tilde{s}) \tag{45}$$

where

$$\tilde{W}(\tilde{z}, \theta) = (\nu\sigma L/a^2) \times \int_0^{2\pi} \mathrm{d}\phi' \int_0^{\pi} \mathrm{d}\theta' \sin\theta' |\mathbf{u} \times \mathbf{u}'| \rho(\tilde{z}, \theta') \tag{46}$$

and $\tilde{V}$ has the same form as (16). Note that the second derivative term with respect to θ, on the right-hand side of eq 13, can now be dropped, approaching the rigid-rod limit. According to (5), the prefactor $\nu\sigma L/a^2 = L\sigma d$ is a-independent, as expected in the rod limit.[46] The solid curve in Figure 6 represents the physical properties deduced from our numerical solution to the above equation set.

Our numerical method for solving eq 45 becomes unstable in small $L\sigma d$ when the self-consistent field $\tilde{W}(\tilde{z},\theta)$ becomes weak. In the extreme case of $L\sigma d = 0$, eq 45 becomes the simplest form of a flux-conservative equation, which has been shown to be numerically unstable, discussed in Chapter 19 of ref 59. Most data shown in Figures 6 and 7 correspond to moderate to large values of $L\sigma d$. We have not yet found a method to deal with the small $L\sigma d$ limit.

Halperin and co-workers considered a model for mobile rod brushes where the grafted end can move freely on the surface of the grafting plane.[46] One can show that this corresponds to an additional $n \ln \sigma$ term in the free energy (3) to account for the translational entropy. The directional ordering of rods are not affected by this extra term. To solve the rod−brush model, Halperin et al. considered a trial function approach, which yielded

$$1 - S_m \propto (L\sigma d)^{-2}, \quad m = 1, 2, 3, \ldots \tag{47}$$

in the large density region $L\sigma d$ for the orientational order parameters. We can also connect $1 - \langle z_{end}\rangle/L$ and $1/2 - \langle z\rangle/L$ to S_1 in the rod limit, which gives

$$1 - \langle z_{end}\rangle/L \propto 1/2 - \langle z\rangle/L \propto 1 - \langle\cos\theta\rangle \propto (L\sigma d)^{-2} \tag{48}$$

The scaling exponent −2 shown above is represented by the long-dashed line in Figure 6, in consistence with the

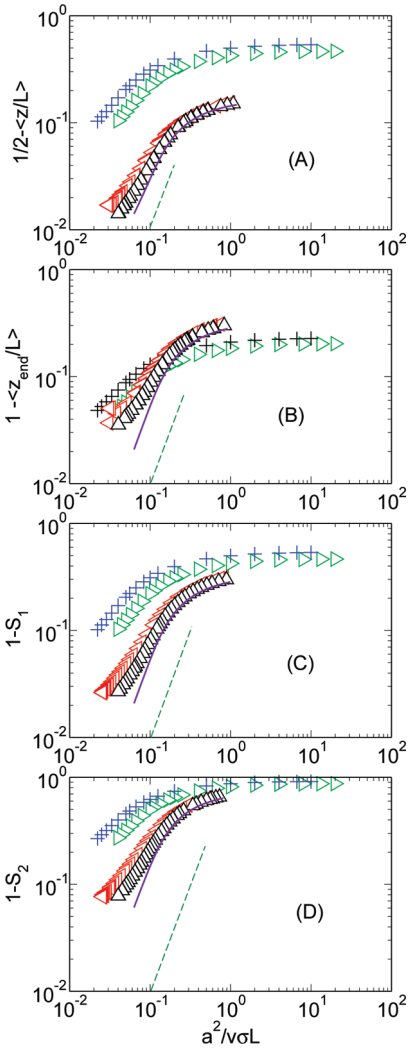

Figure 6. Differences $1/2 - \langle z/L \rangle$, $1 - \langle z_{end}/L \rangle/L$, $1 - S_1$, and $1 - S_2$ as functions of $a^2/\nu\sigma L$ in double-logarithmic plots. Crosses, right triangles, left triangles, and upper triangles represent the numerical results computed from the solution to eq 13 for relative chain length L/a = 1, 0.5, 0.1, and 0.05, respectively. In comparison, the numerical results based on the solution to eq 45, which describes the statistics of a rigid-rod brush, are represented by the solid curve. The dashed line reflects the exponents in power laws (47) and (48).

asymptotic behavior of the solid curve which represents our numerical solution to eq 45.

In the asymptotic region $\nu\sigma L/a^2 \gg 1$, rods are densely grafted and the system can be compared with the bulk nematic liquid crystal phase of lyotropic rods. Odijk deduced the asymptotic scaling behavior for the orientational order parameter,[51] which are also consistent with those discussed by Halperin et al.[46] Furthermore, identifying the volume density $\nu L\sigma/a^2$ with the reduced rod density in Odijk's derivation, we can take the free energy expression from Odijk

$$\beta F - \ln(L/a) = 2\ln(\nu L\sigma/a^2) + ... \qquad (49)$$

The extra $-\ln(L/a)$ term on the left-hand side takes into account an factor of L/a associated with $\bar{Q}$ in (17), which reflects the different scaling in (11) and (43). Note that the free energy is now a logarithmic function of $\nu L\sigma/a^2$ and the coefficient 2 is related to the exponent 2 in power laws (47). In order to verify the asymptotic behavior described in (49), we have replotted the free energy data in Figure 7 in a semi-logarithmic scale. In such a plot, we expect to see a slope of

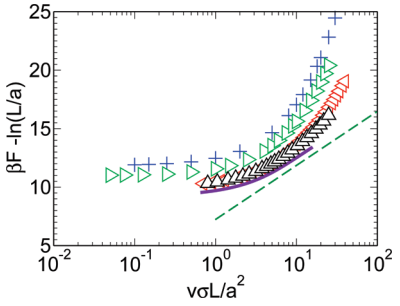

Figure 7. Free energy per chain as a function of $\nu\sigma L/a^2$ in a semilogarithmic plot. Crosses, right triangles, left triangles, and upper triangles represent the numerical results for relative chain length L/a = 1, 0.5, 0.1, and 0.05, respectively. The solid curve corresponds to the solution of the wormlike brush in the rod brush limit, $L/a \ll 1$. The slope of the dashed line describes the prefactor 2 in the asymptotic limit $\nu\sigma L/a^2 \gg 1$ in (49).

2 as the variable $\ln \nu\sigma L/a^2$ becomes large. The long-dashed line in Figure 7 illustrates this limit. The solid curve in the same figure represents the numerical solution to eq 45 and agrees well with the asymptotic behavior in (49).

4. Conclusion

In summary, utilizing the Saito−Takahashi−Yunoki model for a wormlike chain, Onsager-type interaction for the segment−segment interaction, and self-consistent field approach in polymer physics, in section 3 we showed that the physical properties of a wormlike polymer brush depend on two reduced parameters, the ratio between the total chain length L and the effective Kuhn length a, L/a, and a combination of the grafting density σ with the excluded volume per segment ν, $\nu\sigma/a$. This can be compared with the general treatment of a Gaussian chain incorporating an excluded-volume interaction formulated at the level of a second virial approximation, where these two reduced parameters are also reverent. There is an essential difference between these two formalisms: the wormlike brush theory presented in this work not only recovers the physics of now well-establish scaling theory of a Gaussian-chain brush but also establishes physical properties in other parameter regions where a Gaussian brush cannot describe, in particular, the high-grafting region $\nu\sigma/a \gg 1$ as well as near-rigid brushes $a \gg L$.

In the low to moderate grafting density region where $\nu\sigma/a \leq 1$, in section 3.1 we demonstrated that the numerical solution of our formalism recovers the scaling behavior of the conformational properties predicted from the classical-trajectory theory for a Gaussain brush, within the long-chain limit ($L/a \gg 1$). There is a general agreement between the numerical results and power laws predicted from the classical-trajectory theory for the mean end-to-end distance $\langle z_{end} \rangle$, the mean monomer-grafting surface distance $\langle z \rangle$, the orientational order parameter $\langle P_1(\cos\theta) \rangle$, and the free energy per grafted chain F. Our formalism allows us to include directional fluctuations of the wormlike chain, which are ignored previously; as a direct consequence, the scaling behavior of high-order orientational order parameters which can be used to describe the shape of the orientational distribution function, $\langle P_m(\cos\theta) \rangle$ where $m > 1$, have been deduced from the numerical solution.

In the high grafting limit, $\nu\sigma/a \gg 1$, a wormlike brush forms a layer that has the structure resembling a bulk nematic liquid-crystal phase of lyotropic polymers at a similar segmental density. In section 3.2 we showed that the orientational distribution function has a predominant peak at $\theta = 0$, driven by the Onsager interaction. Our numerical data support the scaling relation $1 - \langle z_{end} \rangle/L \propto 1/2 - \langle z \rangle/L \propto 1 - \langle P_m(\cos\theta) \rangle \propto (\nu\sigma/a)^{-2/3}$, originally established for strong nematic ordering in wormlike polymers.[51] One noticeable future of our numerical results is that the data for

the free energy per chain follow the same power law $F \propto (L/a)(\nu\sigma/a)^{2/3}$ in the high grafting limit, similar to the case of weak-to-moderate grafting, a remarkable result that deserves further theoretical investigation.

For a wormlike brush consisting of nearly rigid polymers $a \gg L$ at high grafting density, we showed that another scaling region can be approached. In section 3.3 we showed that our numerical solution closely follows the scaling relation $1 - \langle z_{end}\rangle/L \propto 1/2 - \langle z\rangle/L \propto 1 - \langle P_m(\cos\theta\rangle \propto [\sigma(\nu/a^2)L]^{-2}$, consistent with a previous prediction.[46] In the rod limit, the ratio ν/a^2 is an a-independent parameter, describing the rod diameter. Instead of a power law, the free energy diverges logarithmically as $\sigma(\nu/a^2)L$ increases, which can be compared with that found in a strong bulk nematic phase.[51]

In this work we have focused ourselves on lyotropic wormlike polymers interacting with an Onsager excluded-volume interaction. The basic formalism can be extended to include other relevant physical interactions such as a Maier−Saupe type attraction.[39,42,61,64−66] Within a suitable selection of the interaction parameter, the inclusion of the Maier−Saupe attraction may produce a polymer structure similar to those seen in the bulk liquid crystals, such as a tilted nematic phase. A phase transition between the structure found in this work to a tilted nematic phase may even exist. This is of particular interest in the rod limit where the system can be connected to Langmuir monolayers, where various phases have been theoretically studied.[67,68]

Finally, the formalism developed in this work could also be extended to studying grafted block copolymers with two blocks having different flexibilities, for example, rod and flexible. This can be handled by introducing a path dependent $a = a(s)$ in the theory.[41]

Acknowledgment. We acknowledge the Outstanding Youth Fund (No.20525416), the Program of the National Natural Science Foundation of China (Nos. 20874094 and 50773072), NBRPC (No. 2005CB623800), China Postdoctoral Science Foundation (No. 20080430771), and NSERC (Canada) for financial support as well as SHARCNET for computational time.

References and Notes

(1) Milner, S. T. *Science* **1991**, *251*, 905.
(2) Szleifer, I.; Carignano, M. A. *Adv. Chem. Phys.* **1996**, *94*, 165.
(3) Zhao, B.; Brittain, W. J. *Prog. Polym. Sci.* **2000**, *25*, 677.
(4) Advincula, R. C.; Brittain, W. J.; Caster, K. C.; Rühe, J. *Polymer Brushes: Synthesis, Characterization, Applications*; Wiley-VCH: New York, 2004.
(5) Alexander, S. *J. Phys.* (*Paris*) **1977**, *38*, 983.
(6) de Gennes, P.-G. *Macromolecules* **1980**, *13*, 1069.
(7) Semenov, A. N. *Sov. Phys. JETP* **1985**, *61*, 733.
(8) Milner, S. T.; Witten, T. A.; Cates, M. E. *Europhys. Lett.* **1988**, *5*, 413.
(9) Milner, S. T.; Witten, T. A.; Cates, M. E. *Macromolecules* **1988**, *21*, 2610.
(10) Zhulina, E. B.; Pryamitsyn, V. A.; Borisov, O. V. *Polym. Sci. USSR* **1989**, *31*, 205.
(11) Zhulina, E. B.; Borisov, O. V.; Pryamitsyn, V. A. *J. Colloid Interface Sci.* **1990**, *137*, 495.
(12) Orland, H.; Schick, M. *Macromolecules* **1996**, *29*, 713.
(13) Netz, R. R.; Schick, M. *Macromolecules* **1998**, *31*, 5105.
(14) Likhtman, A. E.; Semenov, A. N. *Europhys. Lett.* **2000**, *51*, 307.
(15) Kreer, T.; Metzger, S.; Muller, M.; Binder, K.; Baschnagel, J. *J. Chem. Phys.* **2004**, *120*, 4012.
(16) Kent, M. S.; Lee, L. T.; Factor, B. J.; Rondelez, F.; Smith, G. S. *J. Chem. Phys.* **1995**, *103*, 2320.
(17) Baranowski, R.; Whitmore, M. D. *J. Chem. Phys.* **1995**, *103*, 2343.
(18) Minko, S.; Muller, M.; Usov, D.; Scholl, A.; Froeck, C.; Stamm, M. *Phys. Rev. Lett.* **2002**, *88*, 035502.
(19) Chakrabarti, A.; Toral, R. *Macromolecules* **1990**, *23*, 2016.
(20) Lai, P.-Y.; Binder, K. *J. Chem. Phys.* **1991**, *95*, 9288.
(21) Lai, P.-Y.; Zhulina, E. B. *J. Phys. II* **1992**, *2*, 547.
(22) Wittmer, J.; Johner, A.; Joanny, J. F.; Binder, K. *J. Chem. Phys.* **1994**, *101*, 4379.
(23) Chen, C.-M.; Fwu, Y.-A. *Phys. Rev. E* **2001**, *63*, 011506.
(24) Murat, M.; Grest, G. S. *Macromolecules* **1989**, *22*, 4054.
(25) Grest, G. S. *Macromolecules* **1994**, *27*, 418.
(26) Liu, H.; Li, M.; Lu, Z.-Y.; Zhang, Z.-G.; Sun, C.-C. *Macromolecules* **2009**, *42*, 2863.
(27) Seidel, C.; Netz, R. R. *Macromolecules* **2000**, *33*, 634.
(28) Muthukumar, M.; Ho, J.-S. *Macromolecules* **1989**, *22*, 965.
(29) Whitmore, M. D.; Baranowski, R. *Macromol. Theory Simul.* **2005**, *14*, 75.
(30) Kim, J. U.; Matsen, M. W. *Eur. Phys. J. E* **2007**, *23*, 135.
(31) Brown, H. R.; Char, K.; Deline, V. R. *Macromolecules* **1990**, *23*, 3385.
(32) Saito, N.; Takahashi, K.; Yunoki, Y. *J. Phys. Soc. Jpn.* **1967**, *22*, 219.
(33) Onsager, L. *Ann. N.Y. Acad. Sci.* **1949**, *51*, 627.
(34) Grosberg, A. Y.; Pachomov, D. V. *Liq. Cryst.* **1991**, *10*, 539.
(35) Cui, S.-M.; Akcakir, O.; Chen, Z. Y. *Phys. Rev. E* **1995**, *51*, 4548.
(36) Chen, J. Z. Y.; Yuan, X.; Sullivan, D. E. *Europhys. Lett.* **2005**, *72*, 89.
(37) Hidalgo, R. C.; Sullivan, D. E.; Chen, J. Z. Y. *Phys. Rev. E* **2005**, *71*, 041804.
(38) Tupitsyna, A. I.; Darinskii, A. A.; Emri, I.; Allen, M. P. *Soft Matter* **2008**, *4*, 108.
(39) Mercurieva, A. A.; Birshtein, T. M.; Amoskov, V. M. *Macromol. Symp.* **2007**, *252*, 90.
(40) Chen, J. Z. Y.; Sullivan, D. E.; Yuan, X.-Q. *Macromolecules* **2007**, *40*, 1187.
(41) Hidalgo, R. C.; Sullivan, D. E.; Chen, J. Z. Y. *J. Phys.: Condens. Matter* **2007**, *19*, 376107.
(42) Jahnig, F. *J. Chem. Phys.* **1979**, *70*, 3279.
(43) Schmid, F.; Schick, M. *J. Chem. Phys.* **1995**, *102*, 2080.
(44) Shim, D. F. K.; Cates, M. E. *J. Phys.* (*Paris*) **1989**, *50*, 3535.
(45) Lai, P.-Y.; Halperin, A. *Macromolecules* **1991**, *24*, 4981.
(46) Halperin, A.; Alexander, S.; Schechter, I. *J. Chem. Phys.* **1987**, *86*, 6550.
(47) Freed, K. F. *Adv. Chem. Phys.* **1972**, *22*, 1.
(48) de Gennes, P.-G. *Scaling Concepts in Polymer Physics*; Cornell University Press: Ithaca, NY, 1993.
(49) Fredrickson, G. H. *The Equilibrium Theory of Inhomogeneous Polymers*; Oxford University Press: New York, 2005.
(50) Khokhlov, A.; Semenov, A. *Physica* **1982**, *112A*, 605.
(51) Odijk, T. *Macromolecules* **1986**, *19*, 2313.
(52) Vroege, G. J.; Odijk, T. *Macromolecules* **1988**, *21*, 2848.
(53) Schena, M.; Shalon, D.; Davis, R. W.; Brown, P. O. *Science* **1995**, *270*, 467.
(54) Seeman, N. C. *Nanotechnology* **1999**, *17*, 437.
(55) Chen, Z. Y. *Macromolecules* **1993**, *26*, 3419.
(56) Chen, Z. Y.; Cui, S. M. *Phys. Rev. E* **1995**, *52*, 3876.
(57) Burkhardt, T. W. *J. Phys. A: Math Gen.* **1997**, *30*, L167.
(58) Chen, J. Z. Y.; Sullivan, D. E. *Macromolecules* **2006**, *39*, 7769.
(59) Press, W. H.; Teukolsky, S. A.; Vetterling, W. T.; Flannary, B. P. *Numerical Recipes in C*, 2nd ed.; Cambridge University Press: New York, 1992.
(60) Laradji, M.; Guo, H.; Zuckermann, M. J. *Phys. Rev. E* **1994**, *49*, 3199.
(61) Kuznetsov, D. V.; Chen, Z. Y. *J. Chem. Phys.* **1998**, *109*, 7017.
(62) He, G. L; Merlitz, H; Sommer, J.; Wu, C. X. *Macromolecules* **2007**, *40*, 6721.
(63) Odijk, T. *Macromolecules* **1983**, *16*, 1340.
(64) Pickett, G. T.; Witten, T. A. *Macromolecules* **1992**, *25*, 4569.
(65) Amoskov, V. M.; Birshtein, T. M.; Pryamitsyn, V. S. *Macromolecules* **1996**, *29*, 7240.
(66) Birshtein, T. M.; Mercurieva, A. A.; Pryamitsyn, V. A.; Polotzkiy, A. *Macromol. Theory Simul.* **1996**, *5*, 215.
(67) Kramer, D.; Ben-Shaul, A.; Chen, Z.-Y.; Gelbart, W. M. *J. Chem. Phys.* **1992**, *96*, 2236.
(68) Somoza, A. M.; Desai, R. C. *J. Phys. Chem.* **1992**, *96*, 1401.